Available online at www.sciencedirect.com
SCIENCE DIRECT®
Control Engineering Practice 14 (2006) 107–120
CONTROL ENGINEERING PRACTICE
www.elsevier.com/locate/conengprac

A novel master switching method for electronic cam control with special reference to multi-axis coordinated trajectory following

Yang-Hung Chang[a], Wei-Hua Chieng[a,*], Chung-Shu Liao[b], Shyr-Long Jeng[c]

[a]*Department of Mechanical Engineering, National Chiao-Tung University, 1001 Ta Hsueh Road, Hsinchu, Taiwan 30010, People's Republic of China*
[b]*R&D Department, Internet Motion Navigator Inc., 8F1, No. 910, Jungjeng Rd., Junghe City, Taipei 235, Taiwan, People's Republic of China*
[c]*Department of Automation Engineering, Ta Hwa Institute of Technology, 1 Ta-Hwa Road, Chiung-Lin, Hsinchu, Taiwan, People's Republic of China*

Received 5 March 2003; accepted 14 January 2005
Available online 19 March 2005

Abstract

Multi-axis coordinated trajectory following is important in CNC machines and metal cutting tools. Recently, flight simulators with electrical actuators have been in increasing demand. However, the coordinate control scheme affects the accuracy of the motion because motors have an insufficient load-capacity relative to the hydraulic actuators. The electronic cam (ECAM) is typically used to perform coordinated control. However, selection of the master may determine potentially very different characteristics of motion. This study proposes an automatic master switching method. The conditions and results of the master switching method for ECAM are detailed. The robustness and stability of the proposed control system is also demonstrated using the well-known structured perturbation analysis tool, μ.

Keywords: Master–slave; Electronic cam; Structured singular value; Robust stability

1. Introduction

The transformation of one of the simple motions, such as rotation, into any other motions is often conveniently accomplished by means of a cam mechanism. A cam mechanism usually consists of two moving elements, the cam and the follower, mounted on a fixed frame. A cam may be defined as a machine element having a curved outline or a curved groove, which, by its oscillation or rotation motion, gives a predetermined specified motion to another element called the follower. The electronic cam (ECAM) is a technique used to perform nonlinear motion electronically similar to that achieved with mechanical cams. ECAM replaces the traditional mechanical cam with a servo-motor and software programmable cam profile.

ECAM tracking is applied to a multi-axis motion control system mainly to enable the slaves to follow consistently trajectories obtained from the predicted sets of reciprocal points of master and slaves. When the master receives a position command, it will or will not be driven to the desired position, and the slaves will be moved into new positions by following the predicted cam profiles. However, in a fixed master ECAM system, the heavily loaded slaves may follow a lightly loaded master, and then the slaves may lose tracking precision as it reaches its current (force) limit. Kim and Tsao (2000) developed an electrohydraulic servo actuator for use in ECAM motion generation, addressing the robust performance control for the fixed slave. Steven (1995) specified a tracking control electronic gearing system called an "optimal feed-forward tracking controller", primarily associated with the fixed slave controller design. Liao, Jeng and Chieng (2004) referred to the

*Corresponding author. Tel.: +886 3571 2121; fax: +886 3572 0634.
E-mail addresses: whc@cc.nctu.edu.tw (Y.-H. Chang), whc@cc.nctu.edu.tw (W.-H. Chieng), admn.imon@msa.hinet.net (C.-S. Liao), bencat@ms15.hinet.net (S.-L. Jeng).

0967-0661/$ - see front matter © 2005 Elsevier Ltd. All rights reserved.
doi:10.1016/j.conengprac.2005.01.012

Nomenclature

E_c input voltage of the servo-motor
G mass center of the cockpit
g gravity acceleration
K_a proportional gain in position loop
K_c AC servo-motor constant (here is 0.0529)
K_n AC servo-motor constant (here is 0.00242552)
L length of linkage
$\mathbf{p}_i$ ith slider position ($i = 1$ to 6)
$\mathbf{q}_i$ ith upper plat ball joint position ($i = 1, 3, 5$)
${}^{O}[q_{xi}\ q_{yi}\ q_{zi}] = {}^{O}\mathbf{O}q_i$ coordinates of $\mathbf{q}_i$ in the frame X–Y–Z–O
${}^{G}[q_{xi}\ q_{yi}\ q_{zi}] = {}^{G}Gq_i$ coordinates of $\mathbf{q}_i$ in the frame x–y–z–G
${}^{Si}[q_{xi}\ q_{yi}\ q_{zi}] = {}^{Si}\mathbf{S}_i\mathbf{q}_i$ coordinates of $\mathbf{q}_i$ in the frame x_i–y_i–z_i–S_i
${}^{Si}[q_{xi}\ q_{yi}\ q_{zi}] = {}^{Si}\mathbf{p}_i$ coordinates of $\mathbf{p}_i$ in the frame x_i–y_i–z_i–S_i
$R(\alpha, \beta, \gamma)$ transformation matrix of Euler angle
$R(\theta_{xi}, \theta_{yi}, \theta_{zi})$ transformation matrix from X–Y–Z–O to x_i–y_i–z_i–S_i ($i = 1, 3, 5$)
$RMS(\bullet)$ root mean square of $\bullet$
s_p lead screw pitch
(S to J) transformation of coordinates from x–y–z–G to x_i–y_i–z_i–S_i
T system sampling time
tr one half the maximum stroke of slider, defined as the distance from the center of guide way to the limit switch
u force applied to slider
X–Y–Z–O inertia coordinate system
${}^{O}[X_G\ X_G\ X_G] = {}^{O}\mathbf{OG}$ coordinate of G relative to the X–Y–Z–O
x–y–z–G cockpit coordinate system
x_i–y_i–z_i–S_i joint coordinate system ($i = 1, 3, 5$) used to represent the positions of slider ball joint p_i and p_{i+1}
τ output torque of AC servo-motor
θ output angle of motor's shaft
$\dot{\theta}$ angular velocity of motor's shaft
ρ distance from O to S_i
$[\alpha\ \beta\ \gamma] = [\phi_x\ \phi_y\ \phi_z]$ Euler angle orientation relative to the x–y–z–G

electronic cam motion generation with special reference to constrained velocity, acceleration and jerk. Each of their control schemes was demonstrated to satisfy the demands of precision and robustness, but to be valid only for its particular application. This study introduces a master switching control scheme, as shown in Fig. 1, to specify the generalized ECAM control problem.

In the master switching control scheme, the most heavily loaded axis must be predetermined before anticipative motion begins: this axis will be treated as the master and the other axes as the slaves. The master may be switched between different types of motion from time to time to exchange the master and one of the slaves in the subsequent action. After the master is instantaneously determined, the next important task is to build ECAM profiles from the demanded ECAM tables. Two curve-fitting methods Dierchx (1993) are proposed to establish piecewise ECAM profile. One is the polynomial curve-fitting method, as shown in Fig. 2, which is suggested for use in cases of low frequency motion. Simulations indicate that the polynomial curve-fitting method (Chen, 1995) (Reich, 1992) performs well, if the frequencies of the active body are less than one-tenth of half of the system's sampling frequency (Nyquist frequency). Restated, this method is favorable if and only if the trajectory of motion is very smooth from the viewpoint of the Nyquist frequency. The second method is the piecewise linear curve-fitting method, as shown in Fig. 3, which is more appropriate for higher frequency motion.

A six degree-of-freedom (DOF) flight simulator SP-120, shown in Figs. 4 and 5, was used to implement and prove the robustness and stability of the proposed master switching control system. Several books and articles help us to comprehend the behavior of the platform. Khalil and Guegan (2002) referred to a novel solution for the dynamic modeling of Gough–Steward manipulators. Lebret, Liu and Lewis (1993) introduced the dynamic analysis and control of a Stewart platform manipulator. Gosselin (1996) referred to a parallel computational algorithm for the kinematics and dynamics of planar and spatial parallel manipulators. Merlet (2000) introduced the analysis of parallel robots. Lazard (1992) referred to the analysis of the Stewart platform and the Gröbner basis. Khalil and Dombre (2002) introduced the modeling, identification and control of robots. Liao, Huang and Chieng (2004) referred to a novel washout filter design for a six degree-of-freedom motion simulator. The important issue of the robust stability of a six DOF flight simulator concerns its six-axis cross-coupled behavior: each axis pulls and drags every other such that the most heavily loaded axis may act unexpectedly; that is, the actual trajectory of the cockpit may be unexpected. This phenomenon follows from inconsistent tracking of the planned trajectory and may cause the cockpit of the flight simulator to leave its nominal workspace. Thus, a robust positioning controller is urgently required. Several articles have referred to the design of controllers of six DOF flight simulators. Chung, Chang and Lin

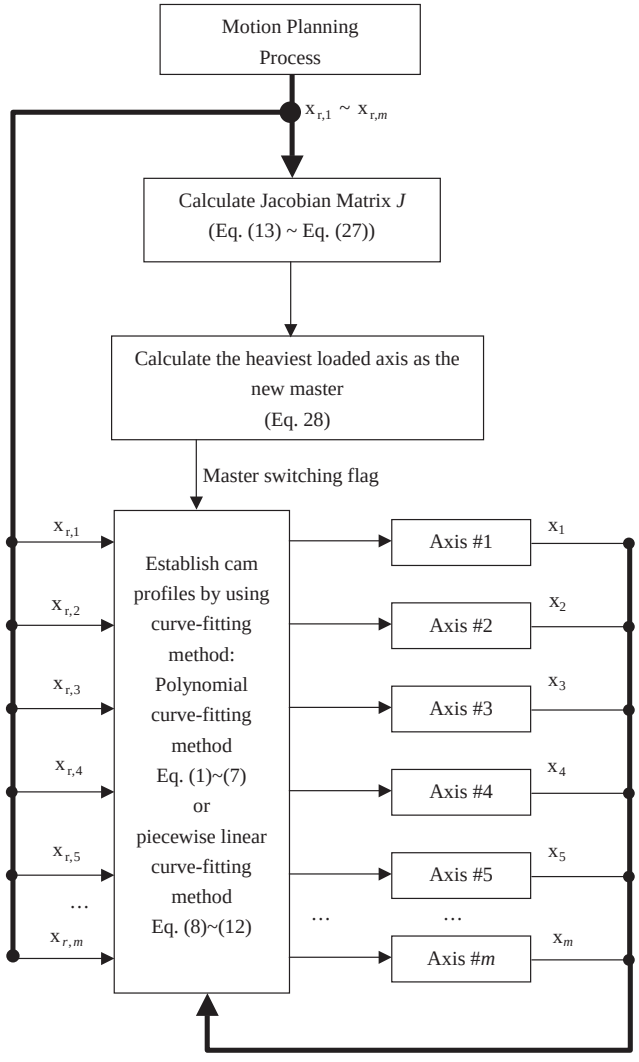

Fig. 1. Master switching method for m-axes ECAM control.

(1999) referred a fuzzy control system for a six DOF simulator and considered the hydraulic actuator system. Werner (1996) introduced a robust tracking control for an unstable plant which was linearized. Plummer (1994) described a nonlinear multi-variable controller for a flight simulator. The procedure for completely designing a robust controller of a nonlinear system consists of finding the nominal controlled plant (Kim & Tsao, 2000; Dixon & Pike, 2002; Zhiwen & Leung, 2002; Al-Muthairi, Bingulac, & Zribi, 2002), which is very complicated and impractical; thus, the dynamics of the nonlinear control system must be linearized and simplified. Simplified dynamics of the simulator SP-120 are proposed to model the structured perturbation with parametric uncertainties. The well-known μ tool (Zhou, 1998) is used to analyze the robust performance of the original control system, and then to demonstrate that it is more robust and stable after the proposed control scheme is applied to the system.

Real-time software was developed to implement the PC-based master switching ECAM control scheme used in the SP-120 flight simulator (Fig. 4). Experimental results show the advantage of the proposed tracking accuracy. However, experimental analysis has also revealed that a shorter system sampling time yields more accurate tracking control, especially when the piecewise linear curve-fitting method is used. It requires a tradeoff between the system sampling time and the calculation burden in a programming cycle.

2. Method of building cam profiles (Master–slaves trajectories)

2.1. Polynomial curve-fitting

A polynomial curve-fitting method is proposed to build a continuous curve in order to fit a known discrete signal, and the established curve is treated as the piecewise-continuous cam profile (master–slaves trajectories). As presented in Fig. 2, T is the sampling time of the driving system and t_{VR} is the period of motion planning. The predictive planned N points are the known discrete commands for which t_{VR} equals N times T; the cam profile of each axis can be expressed as a function of time index t, which describes the common relationship between master and slaves, for $0 \leqslant t \leqslant N \cdot T$, and

$$f_i(t) = \sum_{n=0}^{N-1} c_{i,n} \cdot t^n, \quad i = 0 \text{ to } m \tag{1}$$

in which m is the numbers of axes. By expanding Eq. (1), then

$$\begin{bmatrix} 1 & 0 & \cdots & 0 \\ 1 & T & \cdots & T^{N-1} \\ \cdots & \cdots & \cdots & \cdots \\ 1 & (N-1)T & \cdots & [(N-1)T]^{N-1} \end{bmatrix} \cdot \begin{bmatrix} c_{i,0} \\ c_{i,1} \\ \cdots \\ c_{i,N-1} \end{bmatrix} = \begin{bmatrix} f_i(0) \\ f_i(T) \\ \cdots \\ f_i((N-1)T) \end{bmatrix}$$

$$\Rightarrow T_{matrix} \cdot C_i = F_i$$

$$\Rightarrow C_i = T_{matrix}^{-1} \cdot F_i, \tag{2}$$

where $f_i(t)$ is the position of the ith axis motion planning with respect to time index t, which normally equals the planning time kT, unless an external equivalent force acts on an axis exceeds the critical value, and further, T_{matrix}, C_i and F_i are the constant time matrix, the polynomial parameters of the ith axis and the predicted

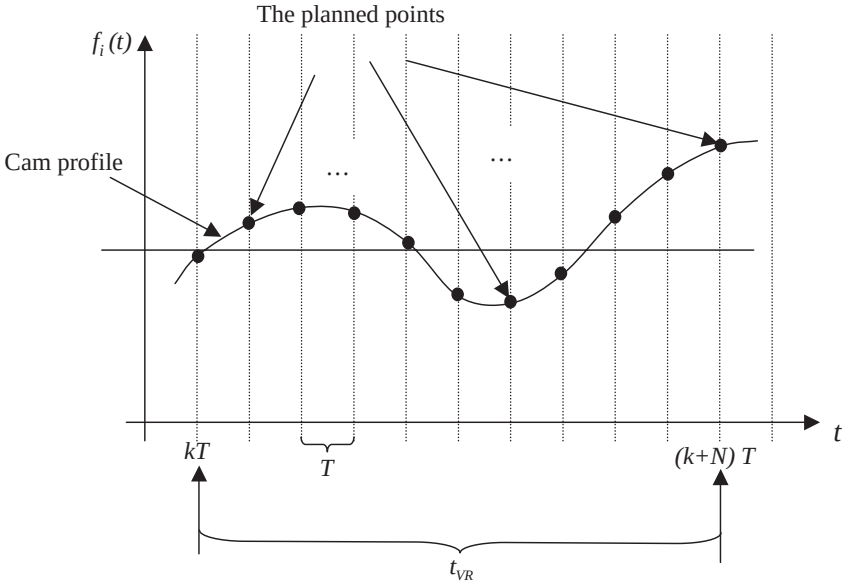

Fig. 2. Cam profile trajectory established using the polynomial curve-fitting method.

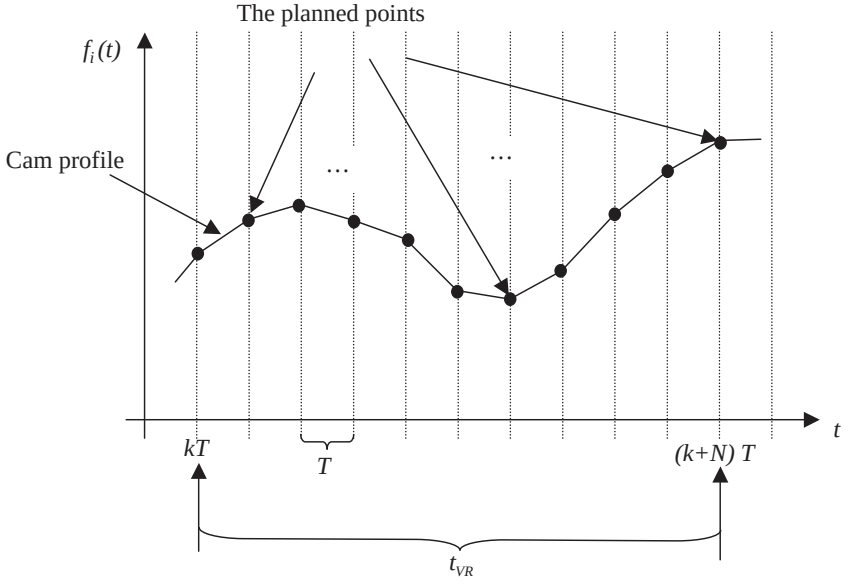

Fig. 3. Cam profile trajectory established using the piecewise linear curve-fitting method.

positions of the ith axis, respectively. The matrix T_{matrix} is constant and nonsingular so T_{matrix}^{-1} exists. Adequately estimating the master's next position $f_{master}(t)$, the position of ith axis processing maximal load, enables the above equation to be used to determine the time index t, and then the estimated positions of all of the slaves are determined by substituting t into Eq. (1). The algorithm includes the following steps.

1. Estimating the next position of the master is an electronic gearing process, and the proper estimate is expressed as follows.

$$f_{master}(\hat{t}_{k+1}) = \hat{x}_{k+1} = x_k + \hat{v}_k \cdot T, \tag{3}$$

where subscript k denotes a real-time counter of time base, $\hat{x}_{k+1}$ is the estimated position of the master; x_k is the present measured position of the master, and $\hat{v}_k$ is

Fig. 4. Prototype SP-120.

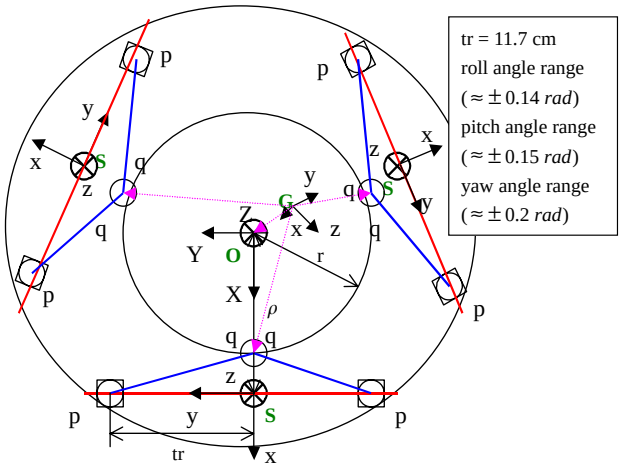

Fig. 5. Vertical view of the simulator platform SP-120.

the velocity estimated during the process of motion planning.

2. Substituting the estimated position $\hat{x}_{k+1}$ of the master into Eq. (1) yields,

$$f_{master}(\hat{t}_{k+1}) = \hat{x}_{k+1} = \sum_{n=0}^{N-1} c_m \cdot \hat{t}_{k+1}^{n}. \tag{4}$$

This equation generally has $N-1$ solutions, and only one real rational solution is correct. A proper constraint $\hat{t}_k < \hat{t}_{k+1} \leqslant (k+1)T$ is added to Eq. (4) to limit the region in which the solution may be found. Sometimes, two solutions satisfy this constraint, but identifying the correct one is not difficult. According to the properties of the polynomial curve and the planned velocities of the master, the sign of the slope of the curve plotted against the time index $\hat{t}_{k+1}$ must be the same as that of the ideal velocity $\hat{v}_k$. For example, in Fig. 6, the solution near $(k+1)T$ is the correct one.

The master velocity in terms of the time index $\hat{t}_{k+1}$ is expressed as

$$f'_{master}(\hat{t}_{k+1}) = \mathrm{d}\hat{x}_{k+1}/\mathrm{d}t = \sum_{n=0}^{N-1} n c_m \cdot \hat{t}_{k+1}^{n-1} \tag{5}$$

such that,

$$\mathrm{sign}\left(\sum_{n=0}^{N-1} n c_m \cdot \hat{t}_{k+1}^{n-1}\right) = \mathrm{sign}(\hat{v}_k), \tag{6}$$

where

$$\mathrm{sign}(\cdot) = \begin{cases} 1 & \text{as } (\cdot) \text{ is positive} \\ -1 & \text{as } (\cdot) \text{ is negative} \\ 0 & \text{as } (\cdot) \text{ is zero} \end{cases}$$

3. The time index is estimated in the preceding steps, and the estimated position of the ith slave is represented as

$$f_{i,slave}(\hat{t}_{k+1}) = \sum_{n=0}^{N-1} c_{i,n} \hat{t}_{k+1}^{n}, \quad i = 1 \text{ to } 5, \tag{7}$$

where $f_{i,slave}(t)$ denotes the position of ith slave axis.

2.2. Piecewise linear curve-fitting

The piecewise linear curve-fitting method is used to fit the signal of higher frequency according to the viewpoint of Nyquist frequency. And then yields a piecewise linear curve as shown in Fig. 3. If the number of motion

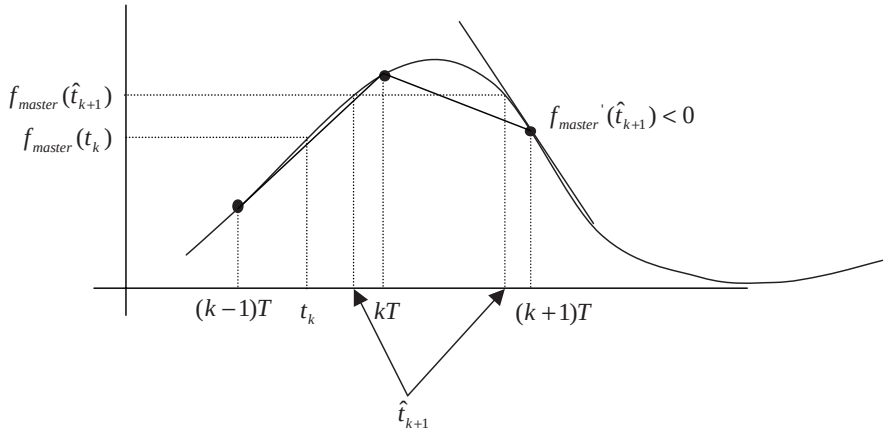

Fig. 6. Conditions on dual solutions using the polynomial curve-fitting method.

planning points equals N, then as in Section 2.1, the cam profile can be expressed as a function of the time index t.

$$f_i(t) = \sum_{n=0}^{N-1} c_{i,n} \cdot |t - nT|, \quad i = 0 \text{ to } m. \tag{8}$$

Expanding Eq. (8) yields

$$\begin{bmatrix} 0 & T & \dots & (N-1)T \\ T & 0 & \dots & (N-2)T \\ \dots & \dots & \dots & \dots \\ (N-1)T & (N-2)T & \dots & 0 \end{bmatrix} \cdot \begin{bmatrix} c_{i,0} \\ c_{i,1} \\ \dots \\ c_{i,N-1} \end{bmatrix} = \begin{bmatrix} f_i(0) \\ f_i(T) \\ \dots \\ f_i((N-1)T) \end{bmatrix}$$
$$\Rightarrow T_{matrix} \cdot C_i = F_i$$
$$\Rightarrow C_i = T_{matrix}^{-1} \cdot F_i, \tag{9}$$

where the parameters in Eqs. (8) and (9) are all defined as in the above section. Similarly, matrix T_{matrix} is constant and nonsingular; thus, T_{matrix}^{-1} exists.

The next time index $\hat{t}_{k+1}$ is properly determined by substituting the estimated position $\hat{x}_{k+1}$ of the master into Eq. (9) and considering the following conditions.

Case 1: $0 \leqslant t_{k+1} \leqslant T$

$$\left(c_0 - \sum_{n=1}^{N-1} c_n\right) t_{k+1} + \sum_{n=1}^{N-1} n c_n T = \hat{x}_{k+1}.$$

Case 2: $T < t_{k+1} \leqslant 2T$

$$\left(\sum_{n=0}^{1} c_n - \sum_{n=2}^{N-1} c_n\right) t_{k+1} + \left(-c_1 + \sum_{n=2}^{N-1} n c_n\right) T = \hat{x}_{k+1}.$$

$\vdots$

Case $N-1$: $(N-2)T < t_{k+1} \leqslant (N-1)T$

$$\left(\sum_{n=0}^{N-2} c_n - c_{N-1}\right) t_{k+1} + \left(-\sum_{n=1}^{N-2} n c_n + (N-1)c_{N-1}\right) T = \hat{x}_{k+1}.$$

Under these conditions, the general formulation is as follows.

$$\hat{t}_{k+1} = \left[\hat{x}_{k+1} + \sum_{n=1}^{N-1} \text{sign}(\hat{t}_{k+1} - nT) c_n \cdot nT\right] \Big/ \sum_{n=0}^{N-1} c_n \times \text{sign}(\hat{t}_{k+1} - nT). \tag{10}$$

This equation is solved first by determining whether the value of $(\hat{t}_{k+1} - nT)$ is positive or negative. Restated, the probable region of $\hat{t}_{k+1}$ must be determined correctly. The region $t_k < \hat{t}_{k+1} \leqslant (k+1)T$ is the correct choice, where t_k is the actual time index obtained by substituting the actual master's position x_k into Eq. (10) at time kT. Multi solutions may be in this region, so the correct solution of Eq. (10) must next be identified. As aforementioned, the sign of the slope of the piecewise linear function of the time index $\hat{t}_{k+1}$ must be the same as that of the ideal velocity $\hat{v}_k$. That is,

$$\text{sign}(\mathrm{d}f(\hat{t}_{k+1})/\mathrm{d}t) = \text{sign}(\hat{v}_k). \tag{11}$$

From the above analysis, the time index $\hat{t}_{k+1}$ can be estimated; then, the estimated position of the ith slave can be represented as

$$f_{i,slave}(\hat{t}_{k+1}) = \sum_{n=0}^{N-1} c_{n,i} \cdot \left|\hat{t}_{k+1} - nT\right|, \quad i = 1 \text{ to } 5. \tag{12}$$

3. Method of determining the master axis

3.1. Applying the proposed control scheme to a six DOF flight simulator

This proposed master switching ECAM control scheme is applied to the control system of multi-axes mechanisms to demonstrate its advantages. In this paper, the six DOF flight simulator SP-120 (Fig. 4) is used to implement the generalized ECAM tracking technique. If the current (force) of the most heavily loaded axis reaches its critical value, then the cockpit cannot easily execute its planned motion easily by directly feeding individual, planned commands to each axis. Rather, the cockpit may sometimes leave its nominal workspace. Accordingly, the master switching ECAM control scheme is better suited than the master fixed ECAM method to this application.

The master of the flight simulator is predetermined the heaviest loaded axis, so the Jacobian matrix (John, 1989) of the simulator must be calculated and updated from time to time. The algorithm for finding the master will be presented as follows.

3.2. Inverse kinematics

Motion-based control may also be called cockpit's positioning control. Cockpit position, including both translation and rotation components, must be transformed into the coordinates of the six sliders using inverse kinematics. The inverse kinematics of the SP-120 motion simulator is as follows.

Fig. 5 presents the top view of SP-120.

$$q_{xi}^2 + (q_{yi} - p_{yi})^2 + q_{zi}^2 = L^2. \tag{13}$$

All of the parameters in Eq. (1) are fixed in the $\mathbf{S}_i$ coordinate system. Thus,

$$\begin{aligned} {}^{Si}\mathbf{S}_i\mathbf{q}_i = {}^{Si}[O_{xi}\ O_{yi}\ O_{zi}]^{\mathrm{T}} + R(\theta_{xi},\theta_{yi},\theta_{zi})\{[X_G\ Y_G\ Z_G]^{\mathrm{T}} \\ + R(\alpha,\beta,\gamma)^G[q_{xi}\ q_{yi}\ q_{zi}]^{\mathrm{T}}\}, \end{aligned} \tag{14}$$

where $R(\alpha,\beta,\gamma)$ is the transformation matrix of the Euler angle, and can be easily expressed as,

$$R(\alpha,\beta,\gamma) = \begin{bmatrix} c\beta c\gamma & -c\beta s\gamma & s\beta \\ s\alpha s\beta c\gamma + c\alpha s\gamma & -s\alpha s\beta s\gamma + c\alpha c\gamma & -s\alpha c\beta \\ -c\alpha s\beta c\gamma + s\alpha s\gamma & c\alpha s\beta s\gamma + s\alpha c\gamma & c\alpha c\beta \end{bmatrix} \tag{15}$$

and $c\beta = \cos\beta, s\alpha = \sin\alpha, \ldots$ and so on, where the above variables and symbols are all presented in the nomenclature.

3.3. Jacobian formulation of simulator SP-120

From Eq. (13),

$$\begin{aligned} &q_{xi}\cdot \mathrm{d}q_{xi}/\mathrm{d}t + (q_{yi} - p_{yi})\cdot \mathrm{d}(q_{yi} - p_{yi})/\mathrm{d}t \\ &\quad + q_{zi}\cdot \mathrm{d}q_{zi}/\mathrm{d}t = 0, \end{aligned} \tag{16}$$

$$\begin{aligned} \mathrm{d}p_{yi}/\mathrm{d}t &= [q_{xi}/(q_{yi} - p_{yi})1q_{xi}/(q_{yi} - p_{yi})] \\ &\quad \times {}^{Si}[\mathrm{d}q_{xi}/\mathrm{d}t\ \mathrm{d}q_{yi}/\mathrm{d}t\ \mathrm{d}q_{zi}/\mathrm{d}t]^{\mathrm{T}} \\ &= [r_{xi}\ r_{yi}\ r_{zi}]\cdot {}^{Si}[\mathrm{d}q_{xi}/\mathrm{d}t\ \mathrm{d}q_{yi}/\mathrm{d}t\ \mathrm{d}q_{zi}/\mathrm{d}t]^{\mathrm{T}}, \\ &\quad i = 1\ \text{to}\ 6, \end{aligned} \tag{17}$$

where $[r_{xi}\ r_{yi}\ r_{zi}] = [q_{xi}/(q_{yi} - p_{yi})1q_{xi}/(q_{yi} - p_{yi})]$; the superscript "T" represents the transpose of the matrix and all the parameters are considered in the $\mathbf{S}_i$ coordinate frame. From Eq. (14)

$$\begin{aligned} &{}^{Si}[\mathrm{d}q_{xi}/\mathrm{d}t\ \mathrm{d}q_{yi}/\mathrm{d}t\ \mathrm{d}q_{zi}/\mathrm{d}t]^{\mathrm{T}} \\ &\quad = R(\theta_{xi},\theta_{yi},\theta_{zi})\{[\mathrm{d}X_G/\mathrm{d}t\ \mathrm{d}Y_G/\mathrm{d}t\ \mathrm{d}Z_G/\mathrm{d}t]^{\mathrm{T}} \\ &\quad + (R_\alpha\cdot \mathrm{d}\alpha/\mathrm{d}t + R_\beta\cdot \mathrm{d}\beta/\mathrm{d}t + R_\gamma\cdot \mathrm{d}\gamma/\mathrm{d}t) \\ &\quad \times {}^G[q_{xi}\ q_{yi}\ q_{zi}]^{\mathrm{T}}\}, \end{aligned} \tag{18}$$

where R_α is the partial derivative of $R(\alpha,\beta,\gamma)$ with respect to α.

$$R_\alpha = \begin{bmatrix} 1 & 0 & 0 \\ c\alpha s\beta c\gamma - s\alpha s\gamma & -c\alpha s\beta s\gamma - s\alpha c\gamma & -c\alpha c\beta \\ s\alpha s\beta c\gamma + c\alpha s\gamma & -s\alpha s\beta s\gamma + c\alpha c\gamma & -s\alpha c\beta \end{bmatrix}$$

R_β is the partial derivative of $R(\alpha,\beta,\gamma)$ with respect to β.

$$R_\beta = \begin{bmatrix} -s\beta c\gamma & s\beta s\gamma & c\beta \\ s\alpha c\beta c\gamma & -s\alpha c\beta s\gamma & s\alpha s\beta \\ -c\alpha c\beta c\gamma & c\alpha c\beta s\gamma & -c\alpha s\beta \end{bmatrix}$$

R_γ is the partial derivative of $R(\alpha,\beta,\gamma)$ with respect to γ.

$$R_\gamma = \begin{bmatrix} -c\beta s\gamma & -c\beta c\gamma & 0 \\ -s\alpha s\beta s\gamma + c\alpha c\gamma & -s\alpha s\beta c\gamma - c\alpha s\gamma & 0 \\ c\alpha s\beta s\gamma + s\alpha c\gamma & c\alpha c\beta s\gamma - s\alpha s\gamma & 0 \end{bmatrix}.$$

Substituting Eq. (16) into Eq. (15) yields

$$\begin{aligned} &[\mathrm{d}p_{yi}/\mathrm{d}t]_{6\times 1} \\ &\quad = [r_{xi}\ r_{yi}\ r_{zi}]\cdot R(\theta_{xi},\theta_{yi},\theta_{zi})\{[\mathrm{d}X_G/\mathrm{d}t\ \mathrm{d}Y_G/\mathrm{d}t\ \mathrm{d}Z_G/\mathrm{d}t]^{\mathrm{T}} \\ &\qquad + (R_\alpha\cdot \mathrm{d}\alpha/\mathrm{d}t + R_\beta\cdot \mathrm{d}\beta/\mathrm{d}t + R_\gamma\cdot \mathrm{d}\gamma/\mathrm{d}t) \\ &\qquad \times {}^G[q_{xi}\ q_{yi}\ q_{zi}]^{\mathrm{T}}\} \\ &\quad = [r_{xi}\ r_{yi}\ r_{zi}]\cdot R(\theta_{xi},\theta_{yi},\theta_{zi})\{[\mathrm{d}X_G/\mathrm{d}t\ \mathrm{d}Y_G/\mathrm{d}t\ \mathrm{d}Z_G/\mathrm{d}t]^{\mathrm{T}} \\ &\qquad \times [R_\alpha\cdot Q_i, R_\beta\cdot Q_i, R_\gamma\cdot Q_i] \\ &\qquad \times [\mathrm{d}\alpha/\mathrm{d}t, \mathrm{d}\beta/\mathrm{d}t, \mathrm{d}\gamma/\mathrm{d}t]^{\mathrm{T}}\}, \end{aligned} \tag{19}$$

where $Q_i = {}^G[q_{xi}\ q_{yi}\ q_{zi}]^{\mathrm{T}}$. However, α, β, and γ are the Euler angles measured in the body embedded coordinate frame, which is the cockpit coordinate system. When dealing with angular velocity, the inertial frame must be the reference frame. Let $[\varpi_x\ \varpi_y\ \varpi_z]^{\mathrm{T}}$ be the cockpit

angular velocity measured in the inertial frame X–Y–Z–O. Then,

$$[\varpi_x\ \varpi_y\ \varpi_z]^{\mathrm{T}} = \begin{bmatrix} 1 & 0 & s\beta \\ 0 & c\alpha & -s\alpha c\beta \\ 0 & s\alpha & c\alpha c\beta \end{bmatrix} \cdot \begin{bmatrix} \mathrm{d}\alpha/\mathrm{d}t \\ \mathrm{d}\beta/\mathrm{d}t \\ \mathrm{d}\gamma/\mathrm{d}t \end{bmatrix} = M \cdot \begin{bmatrix} \mathrm{d}\alpha/\mathrm{d}t \\ \mathrm{d}\beta/\mathrm{d}t \\ \mathrm{d}\gamma/\mathrm{d}t \end{bmatrix}. \tag{20}$$

Therefore

$$[\mathrm{d}\alpha/\mathrm{d}t\ \mathrm{d}\beta/\mathrm{d}t\ \mathrm{d}\gamma/\mathrm{d}t]^{\mathrm{T}} = M^{-1} \cdot [\varpi_x\ \varpi_y\ \varpi_z]^{\mathrm{T}}, \tag{21}$$

where

$$M^{-1} = \begin{bmatrix} c\beta & s\alpha s\beta & -c\alpha s\beta \\ 0 & c\alpha c\beta & s\alpha c\beta \\ 0 & -s\alpha & c\alpha \end{bmatrix} \cdot (c\beta)^{-1}. \tag{22}$$

Substituting Eq. (21) into Eq. (19) yields

$$\begin{aligned}[\mathrm{d}p_{yi}/\mathrm{d}t]_{6\times1} = {} & [r_{xi}\ r_{yi}\ r_{zi}] \cdot R(\theta_{xi}, \theta_{yi}, \theta_{zi}) \\ & \times \{[\mathrm{d}X_G/\mathrm{d}t\ \mathrm{d}Y_G/\mathrm{d}t\ \mathrm{d}Z_G/\mathrm{d}t]^{\mathrm{T}} \\ & + [R_\alpha \cdot Q_i,\ R_\beta \cdot Q_i,\ R_\gamma \cdot Q_i] \\ & \times M^{-1}[\varpi_x\ \varpi_y\ \varpi_z]^{\mathrm{T}}. \end{aligned} \tag{23}$$

According to the definition of Jacobian matrix J, the joint space is converted into Cartesian space, such that,

$$\mathrm{d}X/\mathrm{d}t = J \cdot \mathrm{d}\Theta_i/\mathrm{d}t, \tag{24}$$

where $X_{6\times1} = [X_G\ Y_G\ Z_G\ \alpha\ \beta\ \gamma]^{\mathrm{T}}$, and $\Theta_i = p_{yi}$, $i = 1$ to 6, and

$$\mathrm{d}\Theta_i/\mathrm{d}t = J^{-1} \cdot \mathrm{d}X/\mathrm{d}t. \tag{25}$$

As mentioned above, the angular velocity in the inertial frame is more meaningful than that measured in the body embedded frame. Form Eq. (25), the elements of J^{-1} can be summarized directly as follows.

The first part of Eq. (25) comprises the first three columns of J^{-1}

$$[J_{i1}^{-1}\ J_{i2}^{-1}\ J_{i3}^{-1}] = [r_{xi}\ r_{yi}\ r_{zi}] \cdot R(\theta_{xi}, \theta_{yi}, \theta_{zi}), \quad i = 1\ \text{to}\ 6. \tag{26}$$

The second part of Eq. (25) comprises the last three columns of J^{-1}

$$\begin{aligned}[J_{i4}^{-1}\ J_{i5}^{-1}\ J_{i6}^{-1}] = {} & [r_{xi}\ r_{yi}\ r_{zi}] \cdot R(\theta_{xi}, \theta_{yi}, \theta_{zi}) \\ & + [R_\alpha \cdot Q_i, R_\beta \cdot Q_i, R_\gamma \cdot Q_i] \cdot M^{-1}. \end{aligned} \tag{27}$$

3.4. Calculate the loaded torque of each joint using Jacobian matrix

The relationship between 6×1 joint torque vector $\boldsymbol{\tau}$, $\boldsymbol{\tau} = [\tau_1, \tau_2, \tau_3, \tau_4, \tau_5, \tau_6]$, and the 6×1 equivalent Cartesian force-moment vector $\boldsymbol{F}$, $\boldsymbol{F} = [m\boldsymbol{a}, I_{3\times3}\boldsymbol{\alpha}]$, acting at the mass center of the upper plate, can be written in the form, (John, 1989)

$$\boldsymbol{\tau} = J^{\mathrm{T}}\boldsymbol{F}. \tag{28}$$

4. Analysis of stability and robustness

4.1. Infinity norm of the master switching ECAM controller

The control input of the master switching method can be expressed as $x_r = \Gamma_t \cdot T_{matrix}^{-1} \cdot r$, where r is the reference displacement input. Then, from the characteristics of the master switching ECAM control scheme, the actual speed of each axis theoretically does not exceed its reference speed. Therefore, the reference displacement x_r is confined by $|x_r| \leqslant |r|$; that is, the infinity norm of the controller $(\Gamma_t \cdot T_{matrix}^{-1})$ is confined by

$$||\Gamma_t \cdot T_{matrix}^{-1}||_\infty \leqslant 1. \tag{29}$$

4.2. Stability and robustness

The dynamics of each slider of the SP-120 flight simulator (Figs. 4 and 5) can be modeled by parametric uncertainties, using the linear fractional transformation (LFT) representation. An equivalent mass, m, is introduced to simplify the dynamics of the slider motion and to decouple the components of the system's nonlinear terms, to explicate the stability and the robust performance of the system. Thus, a simplified dynamic model of each slider is

$$\tau = u \cdot 2\pi/s_p = -K_n\dot{\theta} + K_cE_c, \tag{30}$$

where τ is the output torque of AC servo-motor, u is the force applied to slider, s_p is lead screw pitch, K_c is AC servo-motor constant (here is 0.0529), K_n is AC servo-motor constant (here is 0.00242552), E_c is the input voltage of the servo-motor, θ is the output angle of motor's shaft, $\dot{\theta}$ is the angular velocity of motor's shaft, and $x = \theta \cdot s_p/2\pi$ is the displacement of each slider.

$$u = -K_n\dot{x} + K_fK_cE_c, \tag{31}$$

where $K_f = s_p/2\pi$ is the machine constant. As presented in Fig. 7,

$$\ddot{x} = -(c/m)\dot{x} + u/m \tag{32}$$

in which the parameters in Eqs. (30)–(32) are defined in the nomenclature. Suppose that the physical parameters m and c are not known exactly, but are believed to lie in

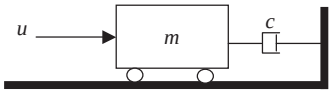

Fig. 7. Equivalent model of slider.

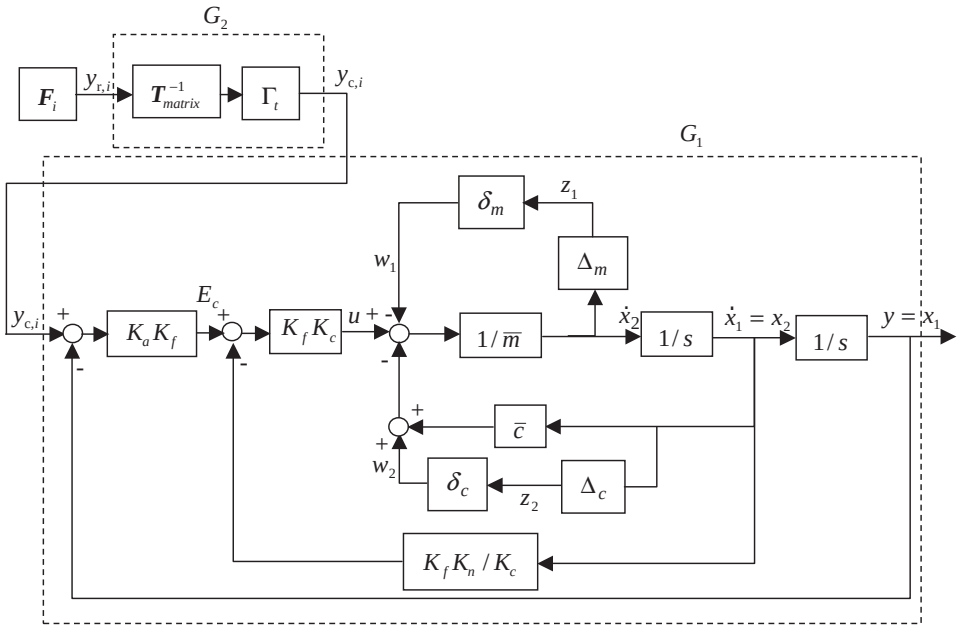

Fig. 8. Simplified control system's block diagram of control system of each slider of simulator SP-120.

known intervals. Assume

$$m = \bar{m} + \Delta_m \delta_m, c = \bar{c} + \Delta_c \delta_c, \tag{33}$$

where the nominal mass is $\bar{m} = (m_H + m_L)/2$, and the nominal damping is $\bar{c} = (c_H + c_L)/2$; the maximum variation of mass is $\Delta_m = (m_H - m_L)/2$, and the maximum variation of damping is $\Delta_c = (c_H - c_L)/2$; the perturbations δ_m and δ_c are confined by $|\delta_m| < 1$ and $|\delta_c| < 1$, respectively, in which $m_H = 250$ kg, $c_H = 15$ kg/s and $m_L = 50$ kg, $c_L = 5$ kg/s are in practice the upper and lower bounds of the slider's nominal mass and damping, respectively.

Fig. 8 presents the system's block diagram according to the foregoing dynamical equations. Suppose the control input is $[w_1, w_2, y_r]^{\mathrm{T}}$ and the output is $[z_1, z_2, y]^{\mathrm{T}}$. Then, using the Doyle's representation, the transformation matrix can be represented as below.

$$M = \left[\begin{array}{cc:ccc} 0 & 1 & 0 & 0 & 0 \\ -K_c K_a/\bar{m} & -(\bar{c} + K_c K_n)/\bar{m} & -1/\bar{m} & -1/\bar{m} & K_c K_a/\bar{m} \\ -\Delta_m K_c K_a/\bar{m} & -\Delta_m(\bar{c} + K_c K_n)/\bar{m} & -\Delta_m/\bar{m} & -\Delta_m/\bar{m} & \Delta_m K_c K_a/\bar{m} \\ 0 & \Delta_c & 0 & 0 & 0 \\ \hdashline 1 & 0 & 0 & 0 & 0 \end{array}\right] = \left[\begin{array}{c:cc} M_{11} & M_{12} \\ \hdashline M_{21} & M_{22} \end{array}\right] \equiv G_1(s) \tag{34a}$$

and

$$G_1(s) = M_{22} + M_{21}(sI - M_{11})^{-1} M_{12} \tag{34b}$$

in which the parameters of Eq. (34a) are defined in the nomenclature, and the system including the perturbations δ_m and δ_c, can be represented using LFT. That is,

$$y = \mathfrak{I}_u(M, \Delta) y_r, \quad \Delta = \begin{bmatrix} \delta_m & \\ & \delta_c \end{bmatrix} \in RH_\infty,$$
$$w = \begin{bmatrix} w_1 \\ w_2 \end{bmatrix} = \Delta \cdot \begin{bmatrix} z_1 \\ z_2 \end{bmatrix} = \Delta \cdot z, \tag{35}$$

where $\mathfrak{I}_u(M, \Delta)$ is the upper LFT, as shown in Fig. 9, and $\Delta \in RH_\infty$ is the structured uncertainty. Stability is often not the only property of a closed-loop system that must be robust to perturbations. The most well-known use of μ as a robustness analysis tool is in the frequency domain. Figs. 10 and 11 show the singular value frequency responses of $G_1(j\omega)$ and the structured singular values, $\mu_\Delta(G_1(j\omega))$, respectively, for each frequency with $\Delta \in C^{2\times 2}$, obtained by adjusting the proportional gain, K_a. These figures are obtained by programming the theorem of μ (Zhao, 2000). Moreover, the bounds of $\mu_\Delta(G_1(j\omega))$ are formulated within the

reference book (Zhou, 1998). In Figs. 10 and 11, the maximum singular value of $G_1(j\omega)$ is increased by decreasing the proportional gain, and the maximum structured singular value is increased by increasing the proportional gain. Table 1 presents the maximum singular values $\|G_1(j\omega)\|_\infty$, the maximum structured singular values $\sup_{\omega\in R}\mu_\Delta(G_1(j\omega))$ and the bandwidth of the control system for various proportional gains. Moreover, if the upper bound of the nominal mass exceeds a critical value, then the maximum structured singular value will be larger than unity, possibly causing the requirement for robust performance to be unsatisfied. Table 2 presents the critical upper bounds of m_H for various proportional gains, K_a. The critical upper bound increases as the proportional gain decreases. Combining Tables 1 and 2 reveals that the system is more robustly stable at a lower proportional gain, but the time constant of the system responses is higher.

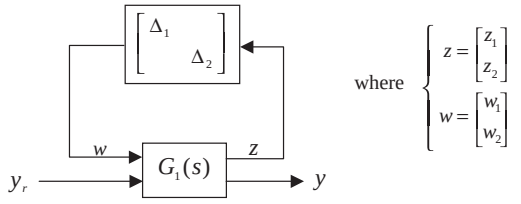

Fig. 9. Upper linear fractional transformation with $\Delta_1 = \delta_m$, $\Delta_2 = \delta_c$ and $|\delta_m| < 1, |\delta_c| < 1$.

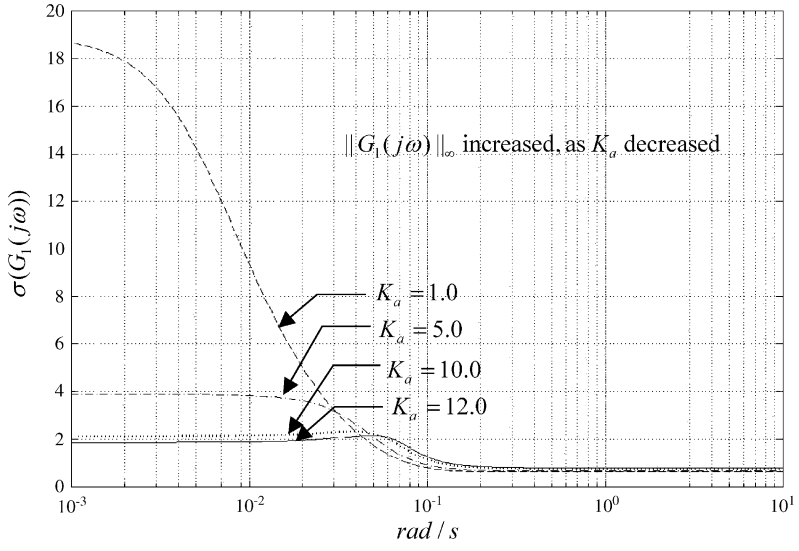

Fig. 10. Singular value frequency responses, $\sigma(G_1(j\omega))$, for various proportional gains, K_a.

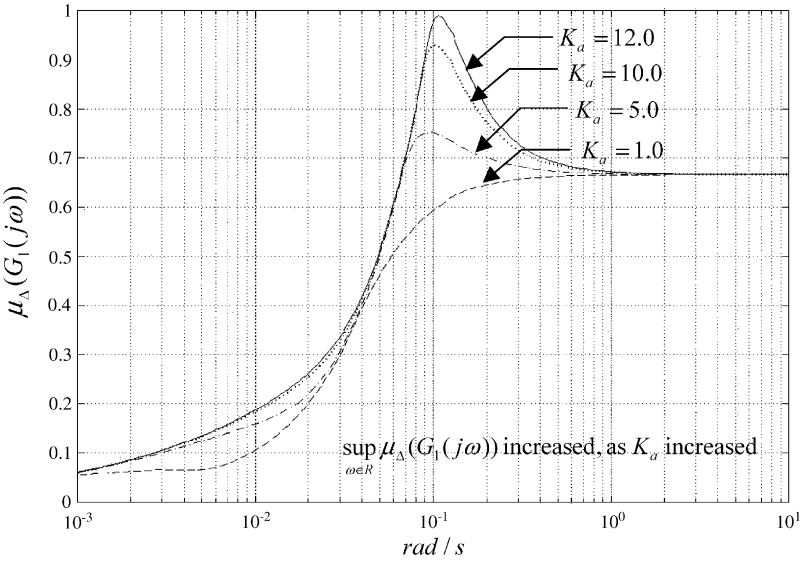

Fig. 11. Upper bounds of structured singular values, $\mu_\Delta(G_1(j\omega))$, for various proportional gains, K_a.

Table 1
Maximum singular values of $||G_1(j\omega)||_\infty$, maximum structured singular values of $\sup_{\omega\in R}\mu_\Delta(G_1(j\omega))$ and bandwidth of control system for various proportional gains, K_a; the upper bound, m_H, of the nominal mass is set to 250 kg

K_a Terms	0.1	1.0	5.0	10.0	12.0
$\|G_1(j\omega)\|_\infty$	88.939455	18.651650	3.910155	2.323414	2.168739
$\sup_{\omega\in R}\mu_\Delta(G_1(j\omega))$	0.666652	0.666658	0.752879	0.929482	0.989907
Bandwidth (rad)	0.00594	0.0188	0.0420	0.0594	0.0651

Table 2
Critical upper bounds of the nominal mass for various proportional gains, K_a

K_a	0.1	1.0	5.0	10.0	12.0
Critical upper bounds (kg)	10,400.0	1414.9	433.6	281.8	254.1

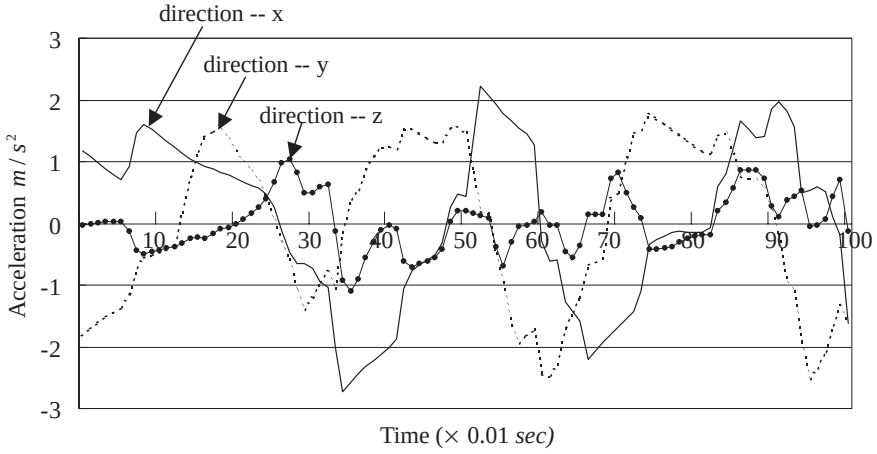

Fig. 12. The piecewise ground earthquake signal involves only the translation.

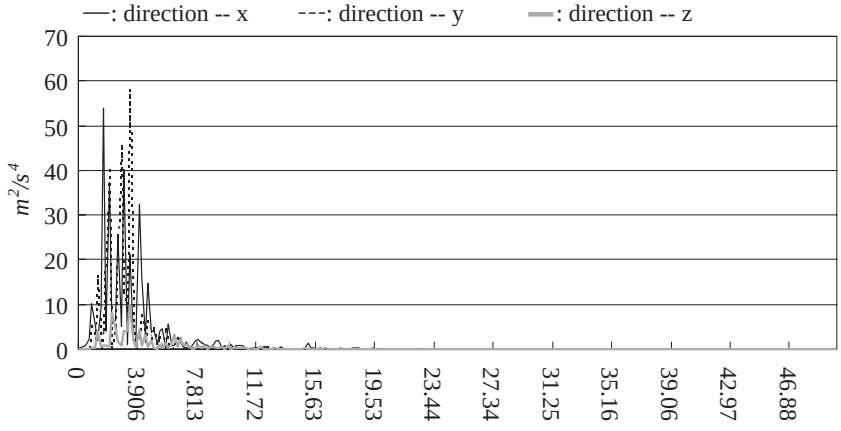

Fig. 13. Power spectrum density of the ground earthquake signal at various frequencies.

Thus, a tradeoff exists between the robustness and the performance of the system's response. Nevertheless, by carefully considering this tradeoff, the most suitable proportional gain can be conveniently adjusted to fit the specific demands of the control. In this paper, m_H is estimated to be around 250 kg by transforming the maximum torque of each joint of the flight simulator SP-120 to the equivalent mass. The maximum torque is

obtained by applying the critical velocity and the maximum tolerable acceleration to drive the slider of the flight simulator provided traveling most the nominal workspace of the simulator. Moreover, for example, if the damping ratio is set to 0.707, then the proportional gain must be adjusted to 6.3, and the maximum structured singular value is then calculated as 0.801358. Clearly, the sufficient and necessary condition

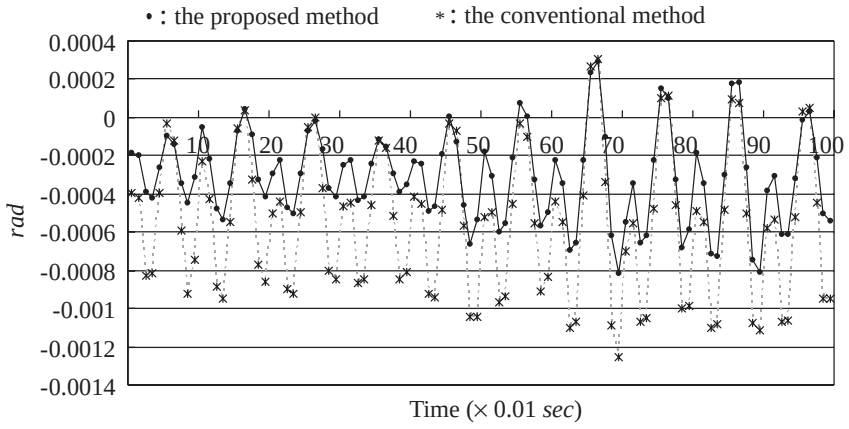

Fig. 14. Comparison of Euler's piecewise roll angle errors obtained using the proposed master switching method with those obtained the conventional method for ECAM control executed on the simulator SP-120.

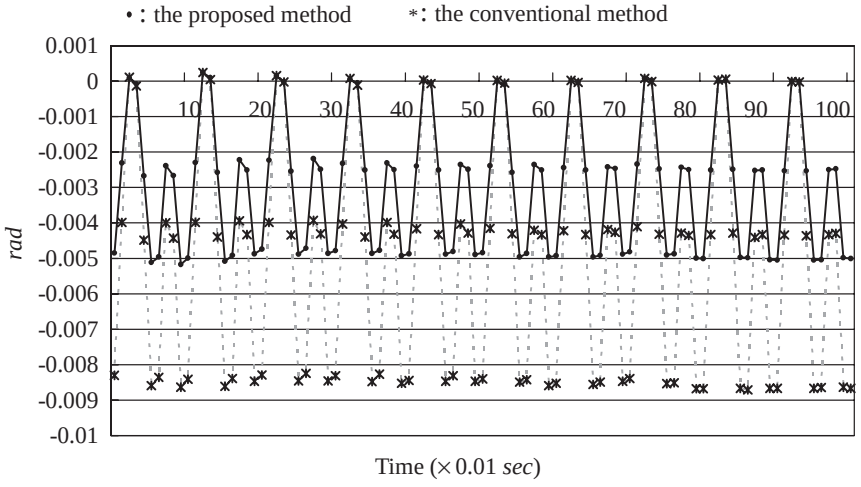

Fig. 15. Comparison of Euler's piecewise pitch angle errors obtained using the proposed master switching method with those obtained the conventional method for ECAM control executed on the simulator SP-120.

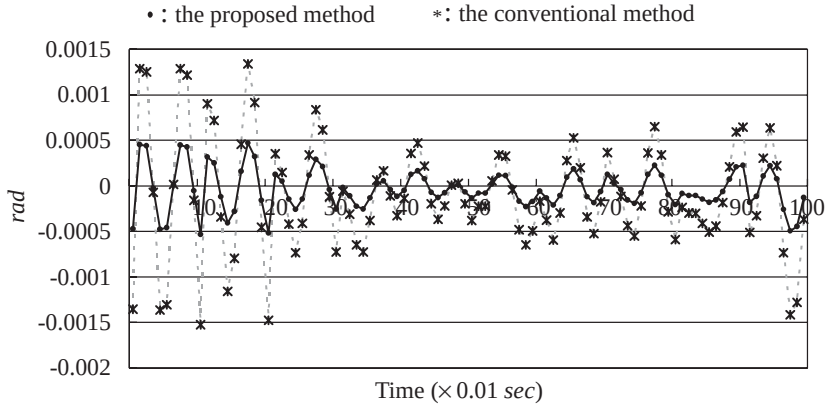

Fig. 16. Comparison of Euler's piecewise yaw angle errors obtained using the proposed master switching method with those obtained using the conventional method for ECAM control executed on the simulator SP-120.

Table 3
Root mean square (RMS) errors of Euler angles, obtained using the proposed master switching method and the conventional method for ECAM control executed on the simulator SP-120

Error items/Tracking method	RMS error of roll (rad)	RMS error of pitch (rad)	RMS error of yaw (rad)
Conventional method	0.0015150	0.003427	0.0004285
Master switching method	0.0007445	0.001988	0.0001499

for robust performance is satisfied. That is, the maximum structured singular value must be less than unity. Consequently, according to the theorem of μ and μ-synthesis, the system is well-defined and internally stable under the structured perturbation, $\|\Delta\|_\infty < 1$.

By combining Eq. (29) with the above results, the maximum structured singular value of the entire system, G_1G_2, is confined by the following inequality:

$$\sup_{\omega\in R}\mu_\Delta(G_1(j\omega)G_2(j\omega)) \leqslant \sup_{\omega\in R}\mu_\Delta(G_1(j\omega)) < 1. \quad (36)$$

Restated, the master switching control system is more robustly stable than the original stable system.

In order to be more convenient for practicing engineers, we make procedures to verify the robustness as in Fig. 17.

5. Experimental results and comparisons

In this study, the proposed ECAM tracking scheme is used on the SP-120 simulator to simulate ground earthquake signal received at Shui-Li Primary School on September 21, 1998. Fig. 12 shows a part of this ground earthquake signal. Fig. 13 presents the power spectrum density of this signal at various frequencies. As aforementioned, the frequencies of the signal are not all less than one-tenth of the Nyquist frequency (here is 50 Hz). Accordingly, piecewise linear curve-fitting method is used in the proposed control scheme.

Figs. 14–16 compare Euler's roll angle errors, the pitch angle errors and the yaw angle errors, respectively, between the conventional and proposed method. This ground earthquake signal involves only the translation; restated, the simulator's output attitude must not include a rotational component. However, as stated above, the six axes may mutually pull and drag each other, causing rotational motion during this pure translation. Table 3 presents the root mean square (RMS) errors of Euler angles for using the proposed ECAM tracking scheme and the master fixed ECAM tracking method executed on the simulator SP-120. In this simulation, the piecewise linear curve-fitting method is used to establish the ECAM profile and the positioning accuracy depends on the system sampling time: a smaller sampling time yields greater accuracy.

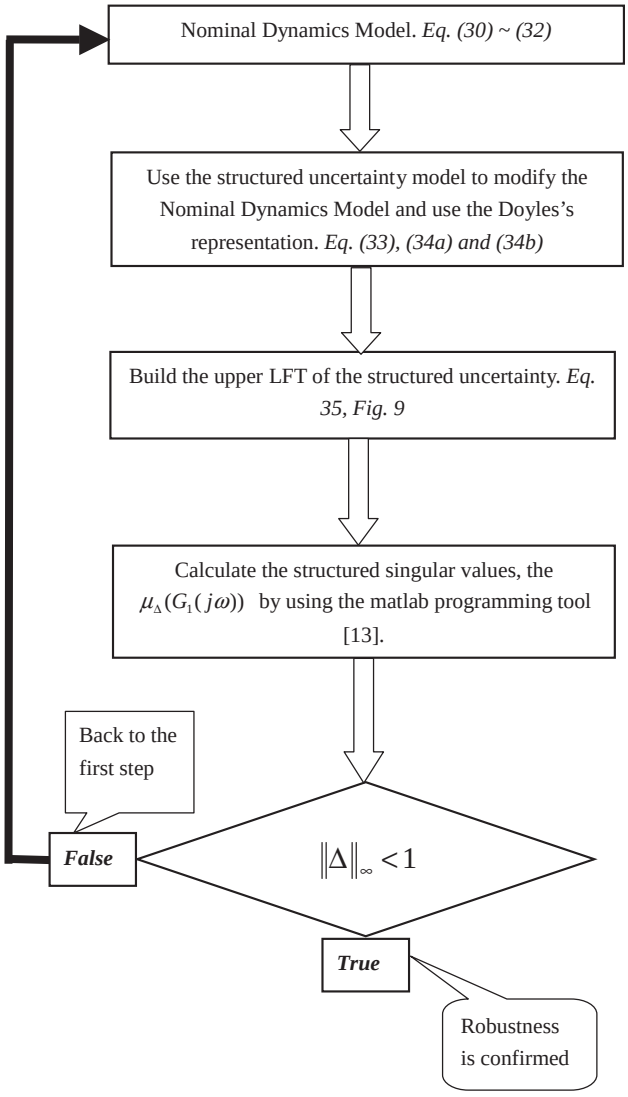

Fig. 17. Procedure of the robustness verification.

However, a tradeoff exists between the calculation time and the system sampling frequency. For example, with a calculation time of around 0.5–1 ms, the system sampling frequency may be set to 100 Hz. Therefore, some small errors still occur (as shown in Figs. 14–16) even if the master switching tracking control is applied to the simulator system. Thus, higher performance computers clearly track more precisely.

6. Conclusion

This study develops an electronic cam control, based on a master switching method, for a flight simulator. The displacement of the slaves of the electronic cam control system depends on the displacement of the master. The master switching method selects the most heavily loaded axis to be the master in real-time during control. As aforementioned, the well-known μ-synthesis of structured uncertainty is used to yield the optimal proportional gain for the overall control system to meet the control performance demands. Furthermore, a piecewise curve-fitting method is introduced, requiring less computational time than conventional polynomial curve fitting, with improved real-time efficiency. The precision and robustness (Fig. 17) of the flight simulator control are crucial concerns and the proposed method is sound.

The structure of the flight simulator in this study has a wide range of applications, such as in a six-axis CNC machine tool. Unlike conventional Cartesian machines, the flight simulator system exhibits six-axis cross-coupled behavior such that each axis pulls and drags every other and the most heavily loaded axis may exceed the load-capacity of the motor-drive system. The master switching method can prevent the load-capacity of the motor-drive system from being exceeded and improve control performance.

Acknowledgement

The authors would like to thank the National Science Council of the Republic of China for financially supporting this research under Contract No. NSC 91-2212-E009-050.

References

Al-Muthairi, N. F., Bingulac, S., & Zribi, M. (2002). Identification of discrete-time MIMO systems using a class of observable canonical-form. *Control Theory and Applications, IEE Proceedings*, *149*(2), 125–130.

Chen, L.-S. (1995). *Follower motion design in a variable-speed cam system*. Institute of Mechanical Engineering, College of Engineering, National Chiao Tung University, T NCTU MEENG, pt.11:3.

Chung, I.-F., Chang, H.-H., & Lin, C.-T. (1999). Fuzzy control of a six-degree motion platform with stability analysis. *IEEE International Conference on Systems*, *1*, 325–330.

Dierchx, P. (1993). *Curve and surface fitting with splines*. Oxford: Oxford University Press.

Dixon, R., & Pike, A. W. (2002). Application of condition monitoring to an electromechanical actuator: A parameter estimation based approach. *Computing & Control Engineering Journal*, *13*(2), 71–81.

Gosselin, C. (1996). Parallel computational algorithms for the kinematics and dynamics of planar and spatial parallel manipulators. *ASME Journal of Dynamic Systems, Measurement and Control*, *118*(1), 22–28.

John, J. C. (1989). *Introduction to robotics mechanics and control* (2nd ed.). Reading, MA: Addison-Wesley Publishing Company, Inc. (pp. 211–215).

Khalil, W., & Dombre, E. (2002). *Modeling, identification and control of robots*, Hermes Sciences Europe.

Khalil, W., & Guegan, S. (2002). A novel solution for the dynamic modeling of Gough–Steward manipulators. *IEEE robotics and automation conference*. Washington DC, USA (pp. 817–822).

Kim, D. H., & Tsao, T.-C. (2000). Robust performance control of electrohydraulic actuators for electronic cam motion generation. *IEEE Transactions on Control Systems Technology*, *8*(2), 220–227.

Lazard, D. (1992). In: ARK (Ed.), *Stewart platform and Gröbner basis*. (pp. 136–142). Ferrare, 7–9 Septembre 1992.

Lebret, G., Liu, K., & Lewis, F. (1993). Dynamic analysis and control of a Stewart platform manipulator. *Journal of Robotic Systems*, *10*(5), 629–655.

Liao, C.-S., Huang, C.-F., & Chieng, W.-H. (2004). A novel washout filter design for a six degree-of-freedom motion simulator. *JSME International Journal Series C*, *47*(2), 626–636.

Liao, C.-S., Jeng, S.-L., & Chieng, W.-H. (2004). Tracking control for electronic cam motion generation with special reference to constrained velocity, acceleration and jerk. *ISA Transactions*, *43*(2), 427–443.

Merlet, J.-P. (2000). *Parallel robots*. Dordrecht: Kluwer Academic Publishers.

Plummer, A. R. (1994). Non-linear control of a flight simulator motion system. *Proceedings of the third IEEE conference on control applications*, *1*, 365–370.

Reich, J.-G. (1992). *C curve fitting and modeling for scientists and engineers*. New York: McGraw-Hill.

Steven, C. C. (1995). *The tracking control for the electric gear system*. National Science Council of the Republic of China, NSC 845-012-011, 1995.

Werner, H. (1996). Robust control of a laboratory flight simulator by non-dynamic multi-rate output feedback. *Proceedings of the 35th IEEE conference on decision and control*, *2*, 1575–1580.

Zhao Qing-Feng, (2000). *Advanced design for automatic control system: using MATLAB programming language* (pp. 1–26). Chan Hwa Science and Technology Book Co. (Chapter 6).

Zhiwen, Z., & Leung, H. (2002). Identification of linear systems driven by chaotic signals using nonlinear prediction. *IEEE transactions on circuits and systems I: fundamental theory and applications*, *49*(2), 170–180.

Zhou, K. (1998). *Essentials of robust control (pp. 55–62, pp. 129–211)*. Upper Saddle River, New Jersey: Prentice-Hall, Inc.